PCCP

Accepted Manuscript




ROYAL SOCIETY OF CHEMISTRY

www.rsc.org/pccp

# Graphene Scavenges Free Radicals to Synergistically Enhance Structural Properties in a Gamma Irradiated Polyethylene Composite Through Enhanced Interfacial Interactions

Elayaraja Kolanthai[1], Suryasarathi Bose[1], K. S. Bhagyashree[2], S.V. Bhat[2], K. Asokan[3], D. Kanjilal[3], Kaushik Chatterjee[1,*]

[1]*Department of Materials Engineering and* [2]*Department of Physics, Indian Institute of Science, Bangalore 560012, India*

[3]*Inter University Accelerator Centre, Aruna Asaf Ali Marg, New Delhi 110067, India*

**author to whom correspondence should be addressed:*

E-mail: kchatterjee@materials.iisc.ernet.in

Ph: +91-80-22933408

## Abstract

A unique strategy to scavenge free radicals in situ on exposure to gamma irradiation in polyethylene (PE) nanocomposites is presented. Blends of ultra high molecular weight PE and linear low density PE (PEB) and their nanocomposites with graphene (GPEB) were prepared by melt mixing to develop materials for biomedical implants. The effect of gamma irradiation on the microstructure and mechanical properties was systematically investigated. The neat blend and the nanocomposite were subjected to gamma ray irradiation in order to improve the interfacial adhesion between PE and graphene sheets. Structural and thermal characterization revealed that irradiation induced crosslinking and increased the crystallinity in the polymer blend. The presence of graphene further enhanced the crystallinity through crosslinks between the polymer matrix and the filler on irradiation. Graphene was found to scavenge the free radicals as confirmed by electron paramagnetic resonance spectroscopy. Irradiation of the graphene containing polymer composites resulted in the largest increases in the modulus and hardness compared to either irradiation or addition of graphene alone to PEB. This work provides new insight into the role of graphene in polymer matrices during irradiation and suggests that irradiated graphene polymer composites could emerge as promising materials for use as articulating surfaces in biomedical implants.


**Keywords:** Ultra-high molecular weight polyethylene; Polyethylene blend; Graphene composite; Gamma ray irradiation; Free radicals

## 1. Introduction

Gamma rays find applications in a wide range of applications such as sterilization of biomedical implants, medical instruments, human blood and food; and in diagnostic imaging and treatment of cancer.[1], [2] In the field of polymer engineering, different kinds of irradiation are frequently used to enhance various properties that are of technological interest such as physico-chemical, structural, electrical and thermal properties, etc.[3], [4] Whereas there are ample literature on the improvement of mechanical properties in polymeric systems, the effect of gamma irradiation on the mechanical properties of nanoparticle filled polymer composites is less understood. Blends of ultra-high molecular weight polyethylene (UHMWPE) and linear low density polyethylene (LLDPE) were chosen as the polymer system in this work to study the effect of graphene and gamma ray irradiation on the mechanical properties of the polymer.

UHMWPE is widely used for preparing acetabular cups and tibial inserts in the human body by virtue of its biocompatibility, low friction coefficient, modulus, toughness and fatigue resistance.[5] However, its low wear resistance limits its applications as a desirable implant material owing to accumulation of wear debris and associated complications such as inflammation, osteolysis, etc.[6] Therefore, polymers with superior mechanical properties are in great demand to develop the next generation prosthetic implants promising longer lifetime especially for more active younger patients.[7] However, it is particularly difficult to process UHMWPE because of its high molecular weight, high melt viscosity and low solubility in solvents. Blending of UHMWPE with a low viscous polymer can offer ease of processing by an industrially viable technique like melt mixing.

LLDPE is a linear semicrystalline polyethylene.[8] Incorporation of LLDPE with other PEs like low density PE (LDPE), high density PE (HDPE) and UHMWPE are envisaged to improve the mechanical properties of the blend.[9] Kyu et al[10] reported that UHMWPE seems to be miscible with LLDPE, HDPE and LDPE in the melt state. Vadhar et al[11] studied the effect of mixing, rheology and mechanical properties of UHMWPE/LLDPE blends. LLDPE is also envisioned to facilitate homogeneous polymerization of UHMWPE and the formation of polymer brush on the folded surfaces of the newly developed polyethylene.[12]

Of late, nanoparticles have been frequently investigated for their role in improving mechanical properties and wear resistance of UHMWPE/LLDPE blend. Park et al[13] reported that UHMWPE/LLDPE-$BaTiO_3$ nanocomposites showed a significant change in mechanical properties. Silicon nitride and alumina nanoparticles in UHMWPE/LLDPE were also reported to improve thermal, dielectric and mechanical properties.[14] In recent years, carbonaceous nanoparticles like carbon nanotubes (CNTs)[15] and graphene oxide (GO),[16] etc. are being explored as reinforcing agents owing to their exceptional mechanical properties and larger surface area. The latter particularly make these materials effective for load bearing orthopedic applications.[17],[18],[19] It has been reported that incorporation of carbonaceous nanoparticles in UHMWPE led to significant strengthening of the composites.[20],[21],[22] The hardness of the GO/UHMWPE composites scaled with increasing GO content in the composites.[23] In our previous work, we have studied the effect of rolling on the evolution of crystallographic texture and mechanical properties of UHMWPE/graphene

and UHMWPE/CNT composites.[24] Graphene was more effective than CNT in improving the modulus prior to rolling.

In the recent past, several strategies have been employed to improve the mechanical properties in polymers and polymer based composites. Irradiation is one such strategy. It is believed to induce scission of the polymer chains and generate free radicals that can lead to the formation of unsaturated cross-links between the adjacent macromolecules.[25] In addition, it has been well established that the mechanical properties of UHMWPE varies with the dosage of gamma ray radiation.[26], [27] Buchanan et al[28] studied the effect of dosage of irradiation on the density and crystallinity of PE. Similar results were also reported in UHMWPE/CNT composites irradiated with gamma rays[21]. However, the mechanical properties of GO/UHMWPE composites irradiated at 90 kGy was shown to be insensitive to the irradiation.[29] Thus, it is now well understood that irradiation can improve the structural properties of UHMWPE.[26] However, the effect of irradiation on graphene/PE based composites have not been studied. Hence, we systematically investigated the effects of gamma rays on the mechanical properties of UHMWPE/LLDPE/graphene composites.

In the present work, UHMWPE/LLDPE blends and with graphene were prepared by melt mixing. The structural, thermal, and mechanical properties of un-irradiated and irradiated samples were characterized using X-ray diffraction (XRD), differential scanning calorimetry (DSC), dynamic thermal analysis (DMA) and micro-hardness tester. In addition, the effect of gamma ray irradiation on the blends and the composites was studied. The free radical formation in the irradiated blends and the composites were studied by electron paramagnetic resonance (EPR) to elucidate the role of graphene in

scavenging the free radicals and synergistically augmenting the mechanical properties of the composites.

## 2. Experimental

### 2.1. Materials

LLDPE of melt flow index (MFI) of 50 g/10 min and density of 0.926 g/cc was obtained from Reliance Industries (Reclair M26500). The UHMWPE ($M_w$ = $3\times10^6$ to $6\times10^6$) was procured from Sigma Aldrich. GO used was prepared by modified Hummer's method using graphite flakes (Superior Company), and reduced graphene oxide (G) via thermal reduction of GO, as previously reported.[30]

### 2.2. Processing of polymer nanocomposites

The neat (70/30 by wt) UHMWPE/LLDPE blend and 1 wt % G were prepared using a conical twin screw mini extruder (Haake Mini lab II) at 220 ºC with a rotating speed of 60 rpm for 20 min under nitrogen environment. Rectangular strips of 25 mm length× 6.5 mm width× 1 mm thickness were produced by hot-pressing using a laboratory scale compression molding machine at 220 ºC for 30 min.

### 2.3. Gamma ray irradiation on polymer samples

The gamma ray irradiation was performed on the neat blend and graphene based composites at room temperature at 1 Pa using a $Co^{60}$ source. The samples were irradiated with two different doses, i.e., 25 and 50 kGy with an average dose rate of 5.5 kGy/h. Fig. 1 represents schematically the preparation of the composite and subsequent irradiation. The neat UHMWPE/LLDPE blend (PEB), the graphene based composites (GPEB), and

the samples with irradiation dosages of 25 and 50 kGy will be hereafter referred to as PEB, GPEB, PEB25, GPEB25, PEB50, and GPEB50.

### 2.4. Characterization

#### 2.4.1 Chemical and morphological analysis

The XRD patterns of un-irradiated and irradiated samples were recorded using a Rigaku Smartlab X-ray diffractometer equipped with a copper source of $CuK_{\alpha}$, A scanning speed of 1 º/min, and a step size of 0.02 º were used to obtain the pattern. Fourier transform infrared (FTIR) spectra were recorded in the range of 550 $cm^{-1}$ to 4000 $cm^{-1}$ with a Bruker Alpha FTIR system using KBr pellets. Raman analysis was carried out on the graphene sheets using a HORIBA, LabRAM HR spectrometer with a 514 nm laser. The morphology of the graphene sheets was also analyzed using FE-SEM (Carl Zeiss Ultra 55) employing a secondary electron mode detector. The samples for scanning electron microscopy were prepared by dispersing them in deionized water using a probe sonicator, and subsequently drop casting them on a silicon wafer. The surface of un-irradiated and irradiated samples and the cryo-fractured surface of extruded strands of PEB and GPEB was characterized using SEM at a low accelerating energy of 5 kV. The solid state carbon 13 nuclear magnetic resonance ($^{13}C$ NMR) spectra of the irradiated composites were recorded at 400 MHz in a Bruker NMR spectrometer operating under a static magnetic field of 9.4 T.

#### 2.4.2 Electron paramagnetic resonance

EPR spectra on un-irradiated and irradiated samples were measured using a Bruker EMX X-Band spectrometer at room temperature with a ER 041X microwave bridge. The microwave frequency, power and modulation frequency were 9.43 GHz, 2.11

mW and 100 kHz, respectively. Rectangular strips (2 × 2 × 6 $mm^3$) weighing 20 mg were used for these measurements. The nature of interactions between the polymer matrix and the graphene sheets in the un-irradiated and irradiated polyethylene blend and graphene based composite was further assessed by refluxing 1.0 g of each sample in boiling xylene (140 ºC) for 10 days using a Soxhlet apparatus.

**2.4.3 Differential scanning calorimetry**

The melting and crystallization behavior of un-irradiated and irradiated samples were analyzed by DSC (Q2000 from TA Instruments). The samples were heated from -50 ºC to 200 ºC at 10 ºC/min. The melting temperature ($T_m$) was measured as the maximum temperature of the endotherm peak. The percentage crystallinity ($X_c$) was calculated from the first heating endotherms using the equation below,

$$X_C = \frac{\Delta H_m}{\Delta H^0_m} \times 100$$

where, $\Delta H^\circ_m$ is the enthalpy of fusion for 100 % crystalline UHMWPE ($\Delta H^\circ_m$ =293 J/g), $\Delta H_m$ is the enthalpy of fusion calculated from the area of endothermic melting peaks.

**2.4.4 Mechanical properties**

The dynamic mechanical behavior of the un-irradiated and irradiated samples was investigated by DMA (Q 800, TA Instruments) under tension mode. The rectangular specimens (25×6.5×1 $mm^3$) were used for measurements. For each sample, the measurement was performed by sweeping the frequency from 0.1 Hz to 100 Hz at room temperature with a preload of 0.01 N and amplitude of 15 μm. Storage modulus and loss modulus were obtained from the DMA data.

The microindentation experiments were performed using a CSM microhardness tester equipped with a Vickers diamond tip. The maximum load used was 100 mN. The

loading and unloading were done at 200 mN/min. The dwell time at maximum load was 5 s. The load-displacement data were acquired in real time by a computer and saved for further analysis. At least six independent indentations were performed for analysis. The hardness (H) was evaluated according to the following equation. [31]

$$H = \frac{P_{max}}{A_{max}} \qquad (1)$$

where, $P_{max}$ is the maximum applied load (in Newton) and $A_{max}$ is the contact area of the indentation at the maximum load ($m^2$). The contact stiffness (S) was determined using the following equation 2 [32]

$$S = \frac{2E_r A_{max}^{1/2}}{\pi^{1/2}} \qquad (2)$$

Where, $A_{max}$ is the surface contact area at the maximum displacement. The reduced elastic ($E_r$) modulus is given by the following equation 3[32]

$$E_r = \beta \frac{\sqrt{\pi}}{2} \cdot \frac{S}{\sqrt{A_{max}}} \qquad (3)$$

Where, β is the correction factor (1.0124 for Vickers indenter) [32]. The elastic modulus ($E_s$) was obtained from the reduced modulus and indenter modulus using equation 4.[31]

$$\frac{1}{E_r} = \frac{(1-\nu_s^2)}{E_s} + \frac{(1-\nu_i^2)}{E_i} \qquad (4)$$

Where, $E_i$, $E_S$ refer to the elastic moduli of the Vicker's indenter (1141 GPa), and the samples respectively, $\upsilon_i$, $\upsilon_s$ the Poisson ratios of the Vicker's indenter (0.07), and the samples (0.46) respectively. [33]

The plasticity index (Ψ) is used to define the relative elastic-plastic behavior of a material which is subjected to external stresses and strains. The plasticity index (Ψ) was calculated using the equation 5.[34]

$$\Psi = \frac{A_P - A_e}{A_p} \qquad (5)$$

where, $A_P$ is the difference between the areas under the loading and unloading curves, and $A_e$ the area under the unloading curve.

## 3. Results and Discussion

### 3.1 Characterization of the nanoparticles

Results from XRD, FTIR, and Raman characterization of GO and G are shown in Figs. 2(a-d). Fig. 2a shows the characteristic diffraction peak for GO at 10.8º (d=8.2 Å) and the diffraction peaks at 25.8º (d=3.45Å) confirming the incomplete exfoliation of the reduced GO.[30] In FTIR spectra, the presence of hydroxyl stretching (3440 $cm^{-1}$), carbonyl stretching (1732 $cm^{-1}$), $sp^2$-hybridized C=C (1627$cm^{-1}$), C-O-C asymmetric stretching (1200-1320 $cm^{-1}$), C-O stretching of phenol or alcohol or ether (1150-1050 $cm^{-1}$) and epoxy C-O-C bending motion (850 $cm^{-1}$) are well evident for GO (Fig. 2b). The carbonyl group along with the phenol or alcohol or ether groups almost disappeared in the spectra upon reduction to G. For the latter, the intensity of hydroxyl stretching peak decreased whereas the peak at 1577 $cm^{-1}$ increased indicating the partial restoration of $sp^2$ bonds. The broad peak at 1132 $cm^{-1}$ was observed due to the C=O vibration, which indicates the reduction of the carboxyl and hydroxyl groups in GO.[35], [36] The G and D bands were obtained at 1601 $cm^{-1}$ and 1359 $cm^{-1}$ for GO in the Raman spectra. The peaks

slightly shifted to lower (G-1589 $cm^{-1}$, D-349 $cm^{-1}$) wave number upon reduction and is consistent with literature (Fig. 2c). SEM image of G showed a typical layered structure (Fig. 2d).

**3.2 Structural characterization of the nanocomposites**

Fig. 3a shows the solid state $^{13}C$ NMR spectra of PEB, PEB50 and GPEB50. In PEB spectrum, a resonance peak at 35.3 ppm and a shoulder at 33.8 ppm corresponds to trans-trans methylene and amorphous phase in the polyethylene blend, respectively[37],[38]. PEB50 and GPEB50 spectra also showed weak resonance peaks. PEB50 showed a small shoulder at 36.8 ppm , which plausibly is due to additional crystallization in polyethylene upon irradiation. In the case of GPEB50, the peak at 35.3 ppm broadened due to increase in the number of carbon atoms by incorporation of graphene in polymer matrix causing the peak to overlap with the shoulder peak. The new resonance peak (indicated by an arrow at 41.2 ppm in Fig. 3b) was related to the carbon-carbon cross-linking in polyethylene by irradiation. In addition, there were two more resonance peaks at 15.4 ppm and 27.5 ppm (indicated by an arrow) due to methyl end groups and radiation induced branching in polymer matrix.[38]

Fig. 4a presents the normalized IR spectra of un-irradiated and irradiated samples. The IR spectra of PEB illustrates four signature bands, namely, the strong CH stretching modes at 2911 $cm^{-1}$ and 2844 $cm^{-1}$, the polyethylene-methylene ($CH_2$) bending mode at 1461 $cm^{-1}$, and the $CH_2$ rocking mode at 719 $cm^{-1}$, which are identical with the characteristic features for PE[39], [40]. In the case of irradiated PEB samples, the additional peak at 965 $cm^{-1}$ is due to trans-vinylene group which indicates the cross-linking between the polymer chains induced by the irradiation [38] ,[41] ,[42] (Fig. 3b).

Additional peaks at 1717 $cm^{-1}$, 1570 $cm^{-1}$ and 1170 $cm^{-1}$ were observed in the IR spectra of GPEB, which indicate the presence of G in the blends. The broad peak between centered around 1170 $cm^{-1}$ indicates the C-O stretching and –C-O-C vibrations of graphene. A small new trans-vinylene peak was observed at 965 $cm^{-1}$ for the irradiated composites (GPEB25 and GPEB50) indicating the cross-linking of the polymer chains.

The un-irradiated and irradiated PEB samples were dissolved in hot xylene to evaluate the effect of irradiation on cross-linking of the polymer chains. The un-irradiated PEB dissolved in hot xylene within a day. In the case of irradiated sample (PEB50) some insoluble residue remained even after 10 days. This may be attributed to the cross-linking between polymer chains upon irradiation (Figs. 4c and 4d). The un-irradiated and irradiated samples of graphene-based composites were dissolved in hot xylene to extract the graphene particles from the composites (Figs. 4e and 4f). This allowed us to study the interactions between the polymer matrix and graphene. Whereas the un-irradiated composite was appreciably soluble as indicated by the visibly suspended graphene (Figs. 4c and 4d), no suspended graphene was seen in the case of the irradiated composites. This is presumably due to the increased interfacial cross-linking between the graphene and polymer matrix induced by irradiation as depicted schematically in Fig 1. As discussed further below, the ability of graphene to scavenge free radicals generated in the polymer matrix during irradiation presumably induces crosslinking between the filler and the polymer chains for enhanced interfacial interactions.

Fig. 5 presents the EPR spectra of un-irradiated and 50 kGy irradiated samples of PEB and GPEB measured at room temperature four months after irradiation to assess the long term presence of free radicals which can dramatically deteriorate the stability and

structural properties of the polymer. Both the irradiated samples, showed a broad peak at ~3400 G. Thus, there was essentially no free radical signal in the two unirradiated samples. This singlet resonance line in the EPR spectra of PEB50 and GPEB50 were obtained for irradiated polymer only when the residual radicals reacted with ambient oxygen. Alternatively, the peroxy radical and an alkoxy radical can react with oxygen to produce the oxygen-induced radicals, which may also show a singlet in the spectra. In general, gamma ray irradiation of polymer generates free radicals, but in this case the free radicals in the polymer might have transformed over time into oxygen centered radicals similar to the findings reported by Oral et al.[43] wherein a sharp singlet was observed in UHMWPE at longer time (≥ 4 months). Importantly, the intensity and width of the singlet peak in the irradiated composite considerably decreased as compared to the irradiated neat blend. This demonstrates that graphene attenuated the level of oxidation putatively as the particles act as radical scavengers in the polymer matrix. An instructive example is the role of MWCNTs in UHMWPE as a radical scavenger thereby reducing the adverse effects of irradiation on polymer degradation as reported by Martinez-Morlanes et al [44]. In a recent study the radical scavenging activity of graphene derived particles was observed.[45] However, the role of graphene as a free radical scavenger in polymer matrices is not reported.

**3.3 Microstructural and thermal characterization of the nanocomposites**

Fig. 6a shows the XRD patterns of neat and gamma ray irradiated samples. The XRD patterns show diffraction peaks at 21.5º, 23.9º and 36.2º corresponding to the (110), (200) and (020) planes, respectively, which are the characteristic peaks of orthorhombic crystal structure of UHMWPE.[46] Besides these peaks, the blend also shows a low

intensity broad peak at 19.4º which is ascribed to the amorphous content in UHMWPE. For LLDPE, diffraction peaks were obtained at the same 2θ position as an orthorhombic phase.[47] Therefore, the peaks appeared broader but phases can be discerned from the pattern. Vadhar et al[11] reported that UHMWPE/LLDPE blend prepared by melt mixing exhibited the broad diffraction peaks in the XRD pattern. On irradiation, intensity of peaks corresponding to (110), (200) and (020) planes increased for PEB with increasing radiation dosage. For composites, addition of 1 wt% G in the blend only served to increase the intensity of the peaks without changing the crystal structure. The percentage crystallinity of un-irradiated and irradiated samples were calculated from XRD data as follows:

% Crystallinity = ((Total area of XRD peak-Amorphous peak area)/Total area) x100.

The calculated values are listed in Fig. 6a. These results indicate that the degree of crystallinity of the polymer blend is enhanced by incorporation of nanoparticles and with increasing dosage of irradiation. The increase in the crystallinity of irradiated PEB may be attributed to the oxidative reaction of radiation-induced radicals. The irradiation of the blend was performed at room temperature and at one atmospheric pressure. The atmosphere oxygen, which can diffuse into the amorphous phase of the polyethylene blend, can react with the alkyl, allyl and polyenyl radicals generating highly reactive and short-lived peroxy radicals. These peroxy radicals might trigger chain scission in the amorphous regions of PEB inducing the formation of additional crystallites. This allows the chains to arrange themselves more easily and pack together resulting in increased crystallinity of the irradiated blend as has been proposed earlier.[48]

In composites, the crystallinity of the polymer matrix increased with both the incorporation of graphene and irradiation. Gamma ray irradiated composites showed higher crystallinity as compared to other samples. It has been already established that the incorporation of G into polymer blend leads to the formation of perfect crystals. This is to merely state that graphene acts as a heterogeneous nucleating site for polymer crystallization and enhance the kinetics of crystallization.[49] Also, gamma irradiation generally leads to chain scission facilitated by oxidative reaction in the amorphous regions. This subsequently leads to the formation of crystallites in the amorphous region due to the generation of free radicals. The free radicals have a high tendency to cross-link with other polymer chains and also with graphene (Figure 1). The latter scavenges the free radicals further resulting in higher crystallinity. A similar mechanism has been proposed for MWCNTs in irradiated PE composites wherein increased crosslinking between the particles and the polymer matrix was observed.[21], [44]

The DSC thermograms of un-irradiated and irradiated samples are shown in Fig. 6b. PEB exhibited a single endothermic peak indicating the co-crystallization between UHMWPE and LLDPE. Similar to the findings by Vadhar et al[11], we conclude that the melt mixing of 70 wt % UHMWPE and 30 wt % LLDPE at 220 ºC led to uniform mixing in the blend. The melting temperature and % crystallinity of un-irradiated and irradiated samples are indicated in Fig 6b. It is obvious from these results that gamma irradiation increased the melting temperature of the PEB because of cross-linking between the polymers chain. The crystallinity of irradiated PEB was found to be higher than that of un-irradiated presumably due to the higher mobility of the new shorter polymer chains induced by molecular chain scission during irradiation as discussed above for XRD

results. A number of studies have observed that irradiation enhances the melting temperature and crystallinity in UHMWPE.[29], [50], [51]

Figs. 7(a-d) compile the SEM micrographs of cryo-fractured surfaces of PEB and the graphene composites before and after irradiation. Two-phase morphology was observed for PEB with LLDPE phase being uniformly dispersed in UHMWPE matrix, which shows fibrillar morphology (Fig. 7a). Irradiation of PEB increased the fibrillar nature (Fig. 7b). Whereas the fractured surface of neat PEB appears smooth, the composite exhibits more pronounced fibrillar morphology (Fig. 7c). Graphene appears well dispersed with no discernable aggregates in the polymer matrix (Fig. 7c). Uniform distribution of the filler and fibrillar morphology are known to enhance improve the mechanical properties. Irradiation did not lead to the loss of fibrillar morphology in the composites, which is known to yield stronger materials (Fig. 7d).

The surface morphology of un-irradiated and irradiated samples was also analyzed (Figs.8a-f). Whereas PEB and GPEB appear smooth with large uneven features resulting from compression molding (Figs. 8a and 8b), irradiated induced a porous morphology in PEB. The fraction of pores seemed to increased with the radiation dosage (Figs. 8c and 8e). The composites, on the other hand, assumed a comparatively smoother surface with minimal surface porosity (Figs. 8d and 8f). This reduced porosity in the composites can be attributed to the protective effect of graphene to the gamma ray radiation. The ability of graphene to scavenge free radicals appears to have minimized damage to the surface of the polymer matrix.

**3.4 Mechanical characterization of the nanocomposites**

Storage modulus measured at 100 Hz from the tensile dynamic mechanical properties of the un-irradiated and irradiated samples are compiled in Fig. 9. The storage modulus of PEB was 532 MPa and increased to 560 MPa upon 50 kGy exposure (PEB50). This increase in the modulus can be traced back to the increased molecular cross-linking and higher crystallinity in PEB as a result of irradiation. The modulus of PEB25 (563 MPa) was slightly higher than PEB50 likely due to the large number of pores which had formed on the surface upon higher irradiation (Fig. 8e). It is generally true that less porosity yields better mechanical properties as porosity causes local discontinuities in the microstructure.

For composites, the storage modulus increased from 532 (PEB) to 599 MPa with the addition of graphene. The increase in modulus was expected on account of the plate-like morphology of graphene. Upon incorporation in the polymer matrix, the large surface area of graphene phase facilitating stress transfer across the graphene-polymer interface. The presence of such interfaces together with inherently high hardness of the graphene results in increased modulus. The uniform distribution of graphene in PEB as indicated by the cryo-fractured morphology (Fig. 7c) and increased crystallinity of the polymer since graphene acts as a heteronucleating site also contribute toward the improvement in modulus of the composites. The storage modulus also increased with radiation dosage, namely, 616 MPa, and 630 MPa with a dosage of 25 kGy, and 50 kGy, respectively. In the case of GPEB the modulus increased monotonically with irradiation unlike in PEB likely because irradiation did not yield pores in the composite. The presence of graphene which scavenges free radicals prevented damage to the polymer matrix minimizing pore formation.

Combination of surface hardness and elastic modulus is often taken to be a qualitative index of wear resistance. Figs. 10a-b depict the plots of load versus displacement for un-irradiated and irradiated blends and composites. The elastic modulus, Vicker's hardness, contact stiffness and plasticity index are summarized in Table 1. The modulus and surface hardness values of PEB were 1.07 GPa and 0.079 GPa, respectively. The hardness of PEB increased with the radiation dosage, which may be attributed to the increased crosslinking. The modulus (1.32 GPa) and hardness (0.137 GPa) of GPEB were appreciably higher than that of PEB. The increase in hardness and modulus of the composites can possibly be due to the uniform distribution of graphene in polymer matrix and the resultant increase in crystallinity, as reported elsewhere[23]. Further, irradiation led to marked increase in the hardness of GPEB (Table 1). Uniform distribution of graphene, enhanced crystallinity, and irradiation-induced cross-linking are the plausible reasons for the enhancement in hardness and modulus.

The contact stiffness was calculated from the slope of the unloading portion of the load-displacement data. The stiffness of polymer increased both due to incorporation of graphene and subsequent irradiation (Table 1). The plasticity index is of particular interest, and it sheds more light on the mechanical properties of polymer-based materials. It is used to characterize the self-healing ability of a material. As given in the Table 1, incorporation of graphene and irradiation caused a significant decrease in plasticity index of the materials. According to Archard's prediction[52], the increased hardness can lower the friction between polymer and metals via minimization of plastic contact area. With the observed marked increase in hardness in the irradiated GPEB, these composites can

be further be explored as candidate materials for use in articulating surfaces for use in biomedical implants.

Carbonaceous particles are believed to exhibit large electron donor-acceptor capacity due to the presence of a network of conjugated double bonds.[29] Similar to graphite, fullerenes, and CNTs known for their ease with which they react with free radicals[53], graphene is also reported to exhibit this characteristic.[45], [54] It was previously reported that carbon lattice in the graphene structure was strongly affected by gamma ray irradiation with variations in their oxygen levels being negligibly low.[29],[55] It was proposed that graphene fillers in their polymeric composites could act as radical scavengers and cross-linking generators upon gamma ray irradiation. Goncalves et al[56] reported on the role of GO as scavenger of radicals generated during polymerization reaction. We hereby propose that the irradiation of the graphene based polyethylene composite enhanced the mechanical properties of the polymer matrix as a result of the following effects. a) the presence of a well dispersed hard filler with large surface areas that facilitates stress transfer; b) the strengthening of the polymer matrix due to the cross-linking of the chains induced by irradiation; c) increased crystallinity of the polymer matrix resulting from the presence of filler which acts as a heteronucleating site and irradiation which induces chain scission and thereby local reorganization of the chains; and d) the enhanced interfacial interactions between the polymer chains with the filler owing to the ability of graphene to scavenge free radicals generated as a result of irradiation that will facilitate better stress transfer to the filler. It is also important to note an additional benefit that the incorporation of graphene can offset the adverse effects of gamma irradiation by minimizing oxidation of the polymer induced by free radicals due

to its free radical scavenging mechanism. EPR results are in good agreement with these conclusions. Thus, incorporation of graphene in irradiated PEB is observed to lead to superior bulk and surface mechanical properties. Hence, the gamma ray irradiated graphene composites can evolve as candidate materials with improved wear resistance.

## 4. Conclusion

UHMWPE/LLDPE blend and with graphene were prepared by melt mixing and thermo-compression, and subsequently subjected to 25 and 50 kGy gamma irradiation at ambient conditions. Irradiation induced cross-linking in the polymer matrix and enhanced the crystallinity in the blend. EPR analysis indicated reduced concentration of radicals suggesting graphene acts as a radical scavenger in the irradiated composites, which can minimize deterioration of the polymer. This also in turn led to the grafting of polymer chains on the filler yielding enhanced interactions at the polymer-graphene interface. The incorporation of graphene thus synergistically increased the modulus and hardness of the composite subjected to irradiation yielding materials that may be better suited as strong and wear resistant materials for use in biomedical implants. These findings should help guide in designing new materials for articulating surfaces in biomedical implants.

## Acknowledgements

This work was funded by the Department of Science and Technology (DST), India. E.K. gratefully acknowledges the Department of Biotechnology, India for the Postdoctoral Research Associate Fellowship. K.C. acknowledges the Ramanujan fellowship from DST.

## References


[1] G. Calais, M. Alfonsi, E. Bardet, C. Sire, T. Germain, P. Bergerot, B. Rhein, J. Tortochaux, P. Oudinot, P. Bertrand, J. Natl. Cancer Inst. 1999, 91, 2081.

[2] K. A. da Silva Aquino, *Sterilization by gamma irradiation,Gamma Radiation*, InTech, 2012.

[3] A. Sionkowska, Prog. Polym. Sci. 2011, 36, 1254.

[4] T. J. Singh, Ganeshsanjeev, K. Siddappa, S. V. Bhat, Journal of Polymer Science Part B: Polymer Physics 2004, 42, 1299.

[5] E. Gomez-Barrena, J.-A. Puertolas, L. Munuera, Y. T. Konttinen, Acta Orthop. 2008, 79, 832.

[6] M. Slouf, S. Eklova, J. Kumstatova, S. Berger, H. Synkova, A. Sosna, D. Pokorny, M. Spundova, G. Entlicher, Wear 2007, 262, 1171.

[7] S. Kearns, B. Jamal, C. Rorabeck, R. Bourne, Clin. Orthop. 2006, 453, 103.

[8] S. L. Sakellarides, A. J. McHugh, Polym. Eng. Sci. 1985, 25, 1179.

[9] A. K. Gupta, S. K. Rana, B. L. Deopura, J. Appl. Polym. Sci. 1992, 44, 719.

[10] T. Kyu, P. Vadhar, J. Appl. Polym. Sci. 1986, 32, 5575.

[11] P. Vadhar, T. Kyu, Polym. Eng. Sci. 1987, 27, 202.

[12] S. Ronca, G. Forte, A. Ailianou, J. A. Kornfield, S. Rastogi, ACS macro letters 2012, 1, 1116.

[13] H. S. Park, J. H. Lee, J.-D. Nam, S. J. Seo, Y. K. Lee, Y. S. Oh, H.-C. Jung, Macromol. Res. 2006, 14, 430.

[14] W. Zhou, C. Wang, T. Ai, K. Wu, F. Zhao, H. Gu, Composites, Part A 2009, 40, 830.

[15] S. Bose, R. A. Khare, P. Moldenaers, Polymer 2010, 51, 975.

[16] P. K. Mural, M. Sharma, G. Madras, S. Bose, RSC Advances 2015, DOI: 10.1039/C5RA02877A.

[17] S. Kumar, S. Bose, K. Chatterjee, RSC Advances 2014, 4, 19086.

[18] S. Kumar, K. Chatterjee, Nanoscale 2015, 7, 2023.

[19] S. Kumar, S. Raj, E. Kolanthai, A. K. Sood, S. Sampath, K. Chatterjee, ACS Appl. Mater. Interfaces 2015, 7, 3237.

[20] P.-G. Ren, Y.-Y. Di, Q. Zhang, L. Li, H. Pang, Z.-M. Li, Macromol. Mater. Eng. 2012, 297, 437.

[21] M. Martinez-Morlanes, P. Castell, V. Martinez-Nogues, M. T. Martinez, P. Alonso, J. Puertolas, Compos. Sci. Technol. 2011, 71, 282.

[22] M. Sturzel, F. Kempe, Y. Thomann, S. Mark, M. Enders, R. Mülhaupt, Macromolecules 2012, 45, 6878.

[23] Z. Tai, Y. Chen, Y. An, X. Yan, Q. Xue, Tribol. Lett. 2012, 46, 55.

[24] E. Kolanthai, R. Kalsar, S. Bose, S. Suwas, K. Chatterjee, Phys. Chem. Chem. Phys. 2014, 16, 23108.

[25] G. Lewis, Biomaterials 2001, 22, 371.
[26] S. M. Kurtz, O. K. Muratoglu, M. Evans, A. A. Edidin, Biomaterials 1999, 20, 1659.
[27] E. Oral, O. K. Muratoglu, NIM B 2007, 265, 18.
[28] F. Buchanan, J. White, B. Sim, S. Downes, J. Mater. Sci.: Mater. Med. 2001, 12, 29.
[29] J. Puertolas, S. Kurtz, J. Mech. Behav. Biomed. Mater. 2014, 39, 129.
[30] P. Xavier, K. Sharma, K. Elayaraja, K. Vasu, A. Sood, S. Bose, RSC Advances 2014, 4, 12376.
[31] W. C. Oliver, G. M. Pharr, J. Mater. Res. 1992, 7, 1564.
[32] A. R. Franco Jr, G. Pintaúde, A. Sinatora, C. E. Pinedo, A. P. Tschiptschin, Materials Research 2004, 7, 483.
[33] D. Bartel, J. Rawlinson, A. Burstein, C. Ranawat, W. Flynn Jr, Clin. Orthop. 1995, 317, 76.
[34] R. Rohini, S. Bose, Phys. Chem. Chem. Phys. 2015, 17, 7907.
[35] N. Wu, X. She, D. Yang, X. Wu, F. Su, Y. Chen, J. Mater. Chem. 2012, 22, 17254.
[36] J. Oh, J.-H. Lee, J. C. Koo, H. R. Choi, Y. Lee, T. Kim, N. D. Luong, J.-D. Nam, J. Mater. Chem. 2010, 20, 9200.
[37] R. Kitamaru, F. Horii, K. Murayama, Macromolecules 1986, 19, 636.
[38] A. L. Cholli, W. M. Ritchey, J. L. Koenig, Appl. Spectrosc. 1987, 41, 1418.
[39] S. Krimm, C. Liang, G. Sutherland, J. Chem. Phys. 1956, 25, 549.
[40] S. A. Umapathi, P. Komaragounder, S. ShailadraKumar, N. S. Kumar, J Bioremed Biodegrad 2012, 3, 1000142 (1.
[41] D. C. Waterman, M. Dole, The Journal of Physical Chemistry 1970, 74, 1913.
[42] O. K. Muratoglu, C. R. Bragdon, D. O. O'Connor, M. Jasty, W. H. Harris, R. Gul, F. McGarry, Biomaterials 1999, 20, 1463.
[43] E. Oral, S. L. Rowell, O. K. Muratoglu, Biomaterials 2006, 27, 5580.
[44] M. Martinez-Morlanes, P. Castell, P. Alonso, M. T. Martinez, J. Puértolas, Carbon 2012, 50, 2442.
[45] Y. Qiu, Z. Wang, A. C. E. Owens, I. Kulaots, Y. Chen, A. B. Kane, R. H. Hurt, Nanoscale 2014, 6, 11744.
[46] H. Kiho, A. Peterlin, P. H. Geil, J. Appl. Phys. 1964, 35, 1599.
[47] K. A. Moly, H. J. Radusch, R. Androsh, S. S. Bhagawan, S. Thomas, Eur. Polym. J. 2005, 41, 1410.
[48] M. Shafiq, M. S. Mehmood, T. Yasin, Mater. Chem. Phys. 2013, 143, 425.
[49] J. Liang, Y. Huang, L. Zhang, Y. Wang, Y. Ma, T. Guo, Y. Chen, Adv. Funct. Mater. 2009, 19, 2297.
[50] M. Goldman, R. Gronsky, R. Ranganathan, L. Pruitt, Polymer 1996, 37, 2909.

[51] S. M. Lee, H.-J. Jeon, S. W. Choi, H. H. Song, Y. C. Nho, K. Cho, Macromol. Res. 2006, 14, 640.
[52] S. Ge, S. Wang, X. Huang, Wear 2009, 267, 770.
[53] A. Galano, Nanoscale 2010, 2, 373.
[54] P. A. Denis, J. Phys. Chem. C 2009, 113, 5612.
[55] A. Anson-Casaos, J. A. Puertolas, F. J. Pascual, J. Hernandez-Ferrer, P. Castell, A. M. Benito, W. K. Maser, M. T. Martinez, Appl. Surf. Sci. 2014, 301, 264.
[56] G. Goncalves, S. M. A. Cruz, A. Ramalho, J. Gracio, P. A. A. P. Marques, Nanoscale 2012, 4, 2937.

Table 1 Mechanical properties of un-irradiated and irradiated PEB and GPEB

| **Sample code** | **Vicker's hardness (GPa) × $10^{-1}$** | **Elastic modulus (GPa)** | **Contact stiffness (mN/μm)** | **Plasticity index (Ψ)** | **% change in ( Ψ)[a]** |
|---|---|---|---|---|---|
| **PEB** | 0.79±0.05 | 1.07±0.08 | 51.49±2.35 | 0.43±0.02 | - |
| **PEB25** | 0.92±0.06 | 1.25±0.22 | 53.43±1.02 | 0.41±0.17 | 4.7 |
| **PEB50** | 1.05±0.06 | 1.28±0.21 | 57.67±2.39 | 0.40±0.12 | 7.0 |
| **GPEB** | 1.37±0.12 | 1.32±0.15 | 59.73±1.28 | 0.35±0.05 | 19.7 |
| **GPEB25** | 1.40±0.09 | 1.48±0.07 | 61.58±2.37 | 0.31±0.04 | 28.0 |
| **GPEB50** | 1.55±0.16 | 1.58±0.32 | 65.53±1.25 | 0.25±0.08 | 47.9 |

[a] with respect to un-irradiated PEB samples

## Figure captions

**Fig.1** Schematic representation for preparation of the nanocomposite subjected to irradiation yielding a cross-linked composite and enhanced interfacial interactions between the polymer chains and the filler in the composite.

**Fig.2** Characterization of GO and G: (a) XRD patterns, (b) FTIR spectra, (c) Raman spectra and (d) SEM micrograph of G

**Fig.3** $^{13}C$ NMR spectra of of PEB, PEB50 and GPEB50 (a) normalized intensity full spectra and (b) magnified spectra.

**Fig.4** FTIR spectra of (a) un-irradiated and gamma ray irradiated samples of PEB and GPEB and (b) magnified spectra in the 940-990 $cm^{-1}$ range (c, d, e, f) Photographs of vials showing PEB, PEB 50, GPEB and GPEB50 extracted in hot xylene.

**Fig.5** X-band (mass normalized) EPR spectra of un-irradiated and 50 kGy irradiated PEB and GPEB

**Fig.6** (a) XRD patterns and (b) DSC thermogram of first heating melting curve of un-irradiated and gamma ray irradiated PEB and GPEB. $T_m$ from DSC and % crystallinity from DSC and XRD are indicated for each plot.

**Fig.7** SEM micrographs of the cryo-fractured surface of (a) PEB, (b) PEB50, (c) GPEB, (d) GPEB50

**Fig.8** SEM micrographs of (a) PEB, (b) GPEB, (c) PEB25, (d) GPEB25, (e) PEB50 and (f) GPEB50 showing surface damage (porosity) from irradiation

**Fig.9** (a) Storage modulus at 100 Hz from DMA measurements of unirradiated and irradiated PEB and GPEB

**Fig.10** Representative microindentation load-displacement curves of un-irradiated and irradiated (a) PEB and (b) GPEB.

**Fig. 1**

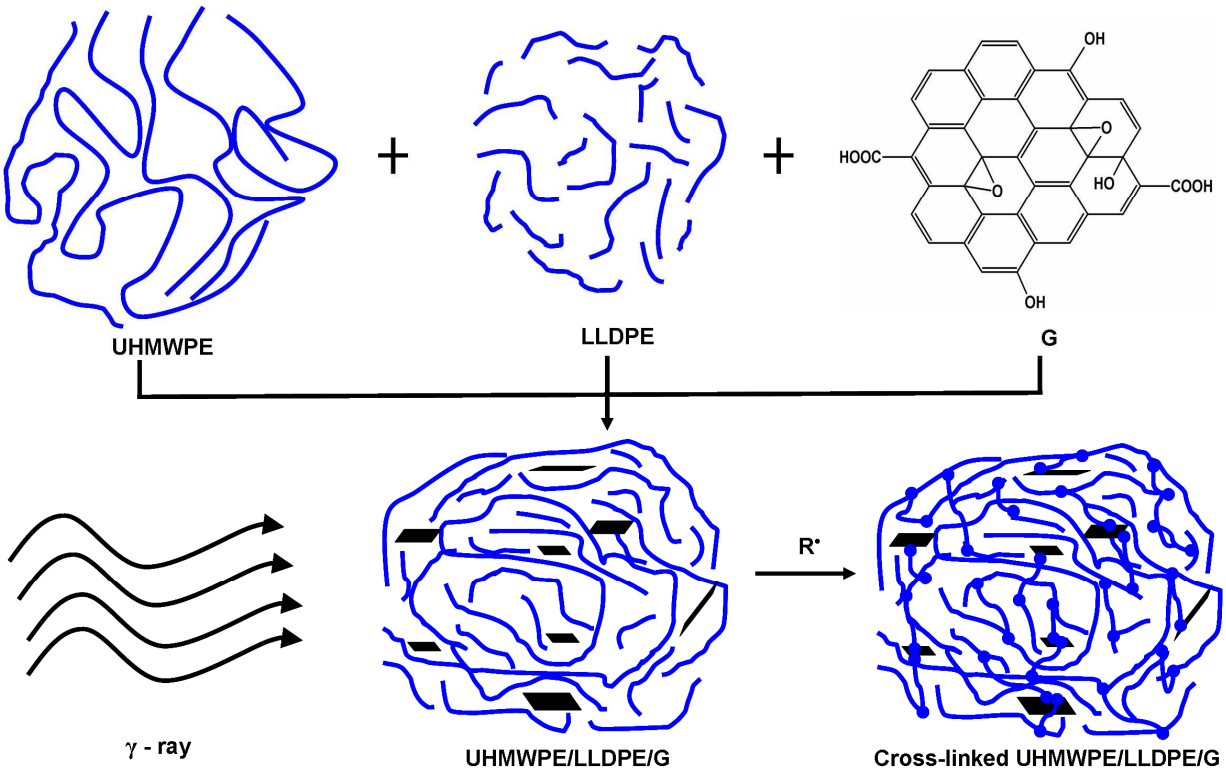

**Fig. 2**

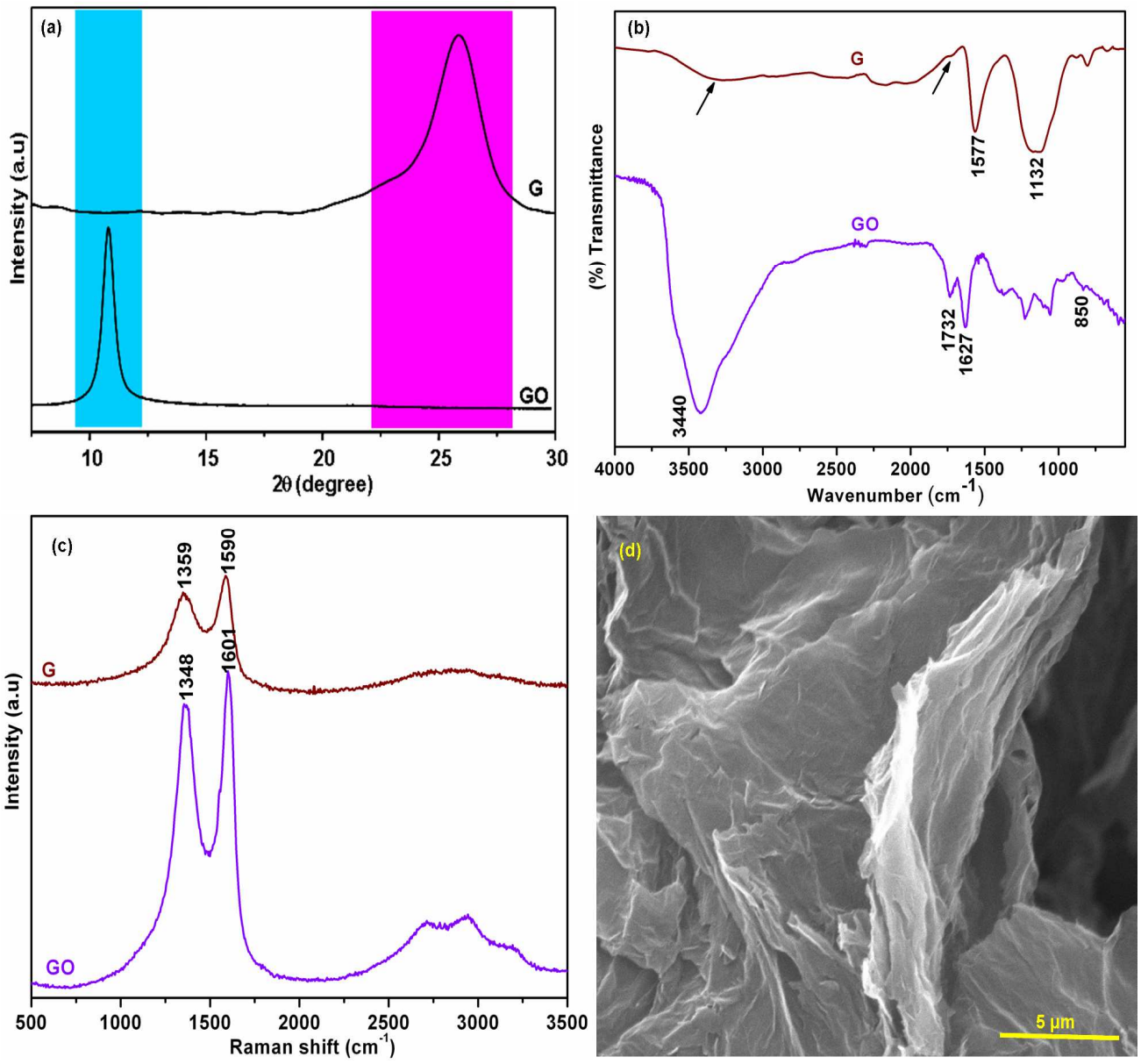

**Fig. 3**

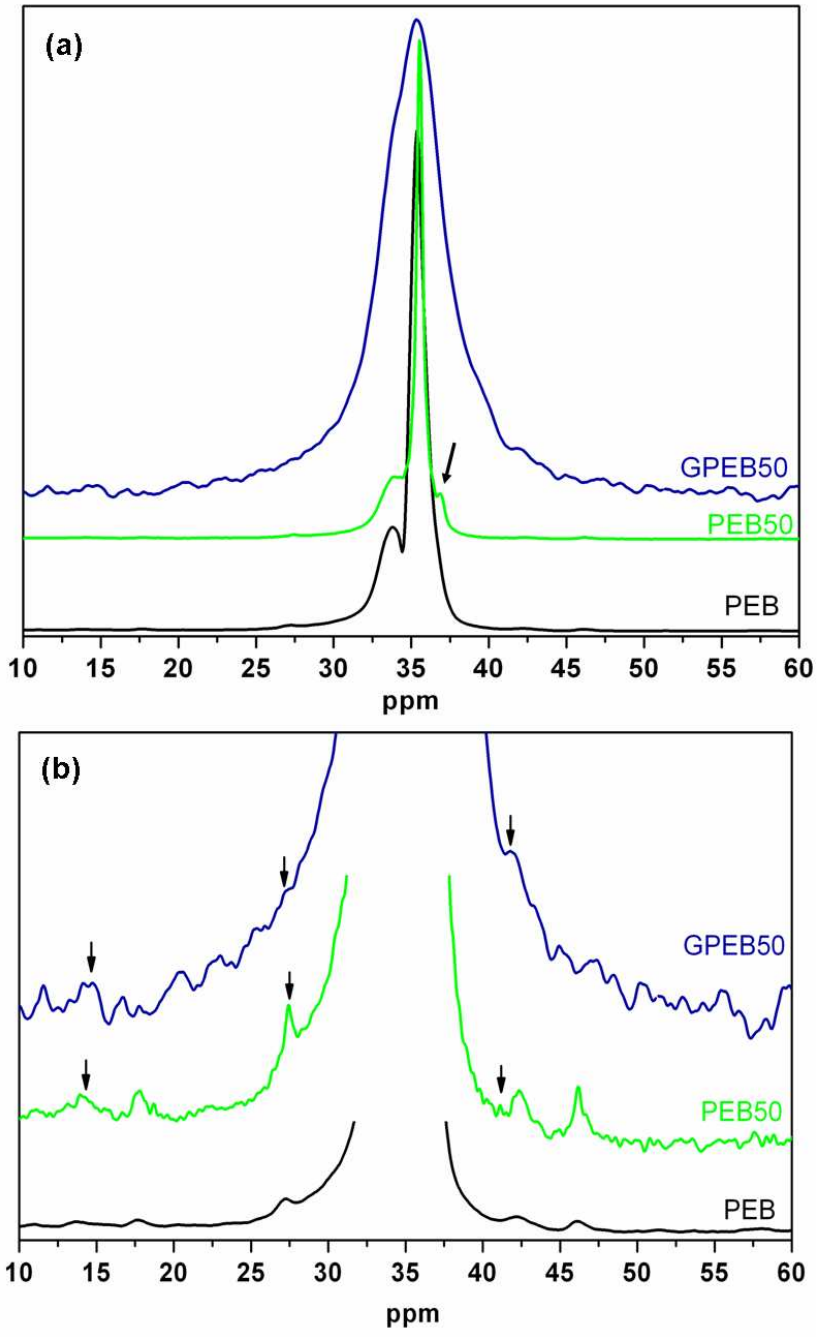

**Fig. 4**

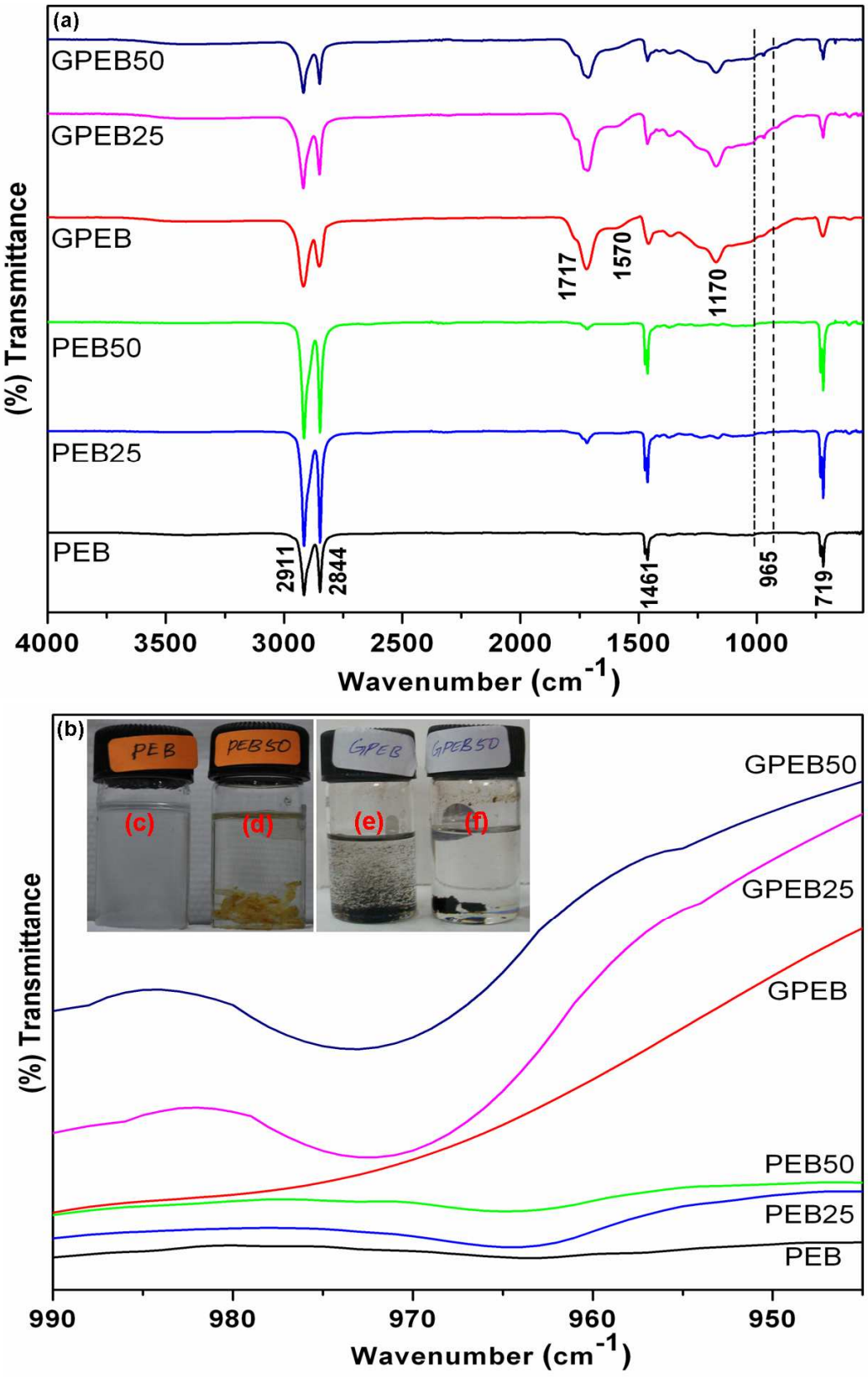

**Fig. 5**

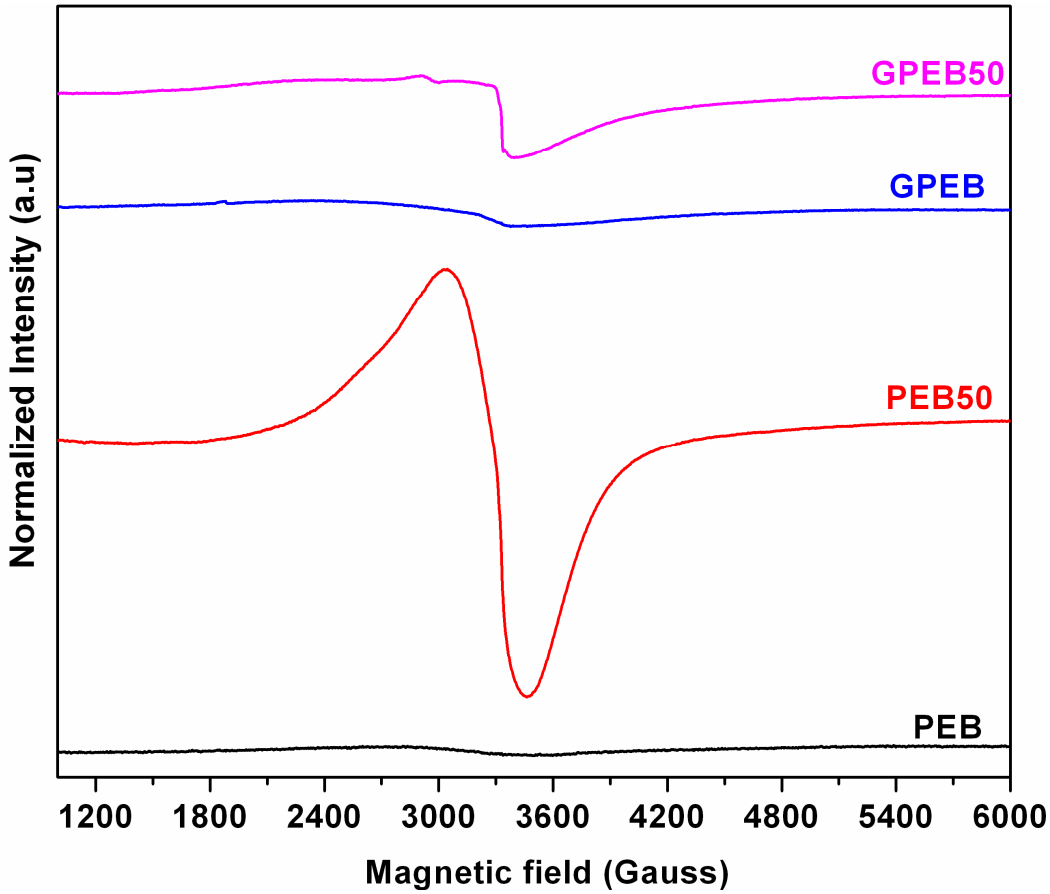

**Fig. 6**

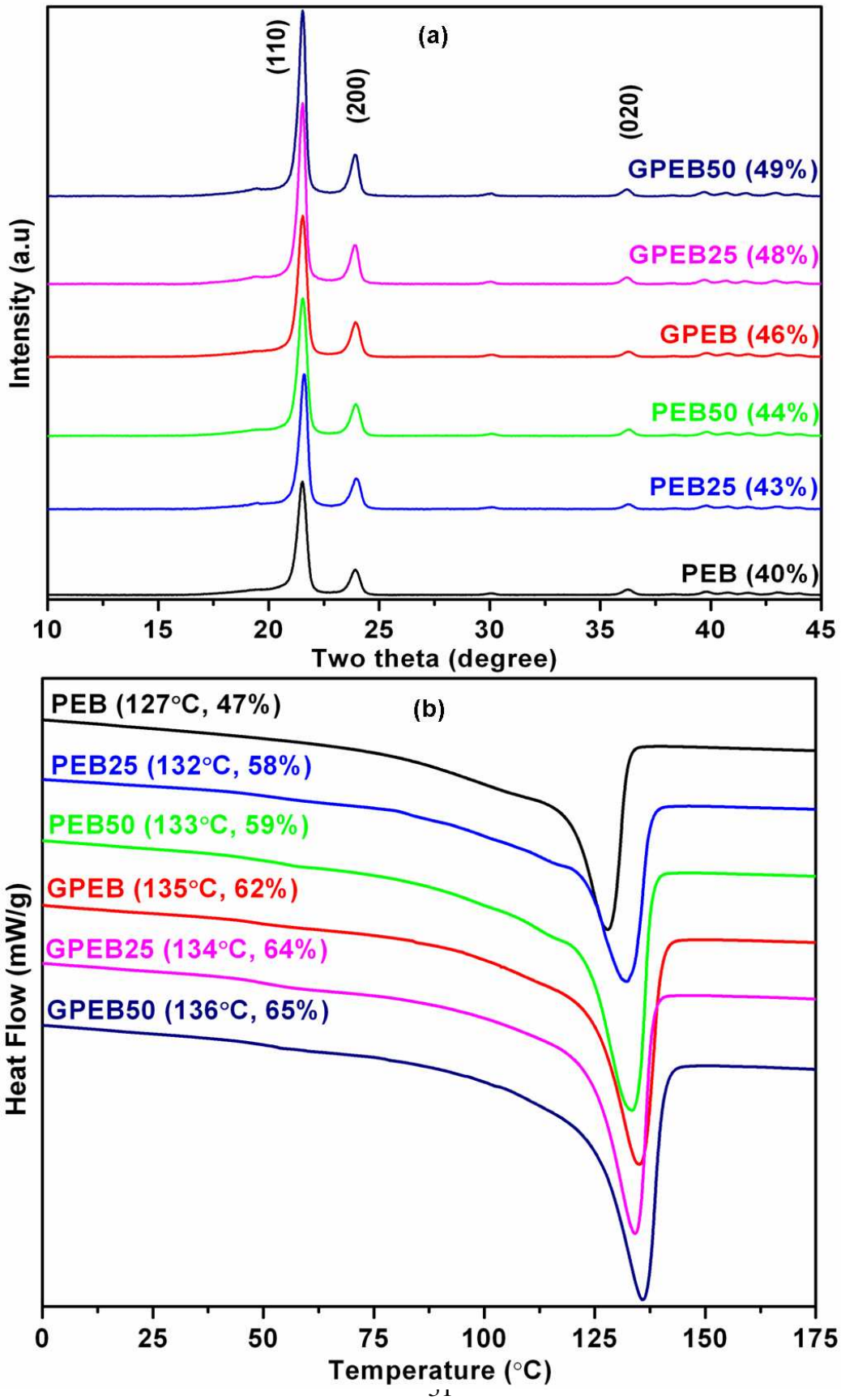

**Fig. 7**

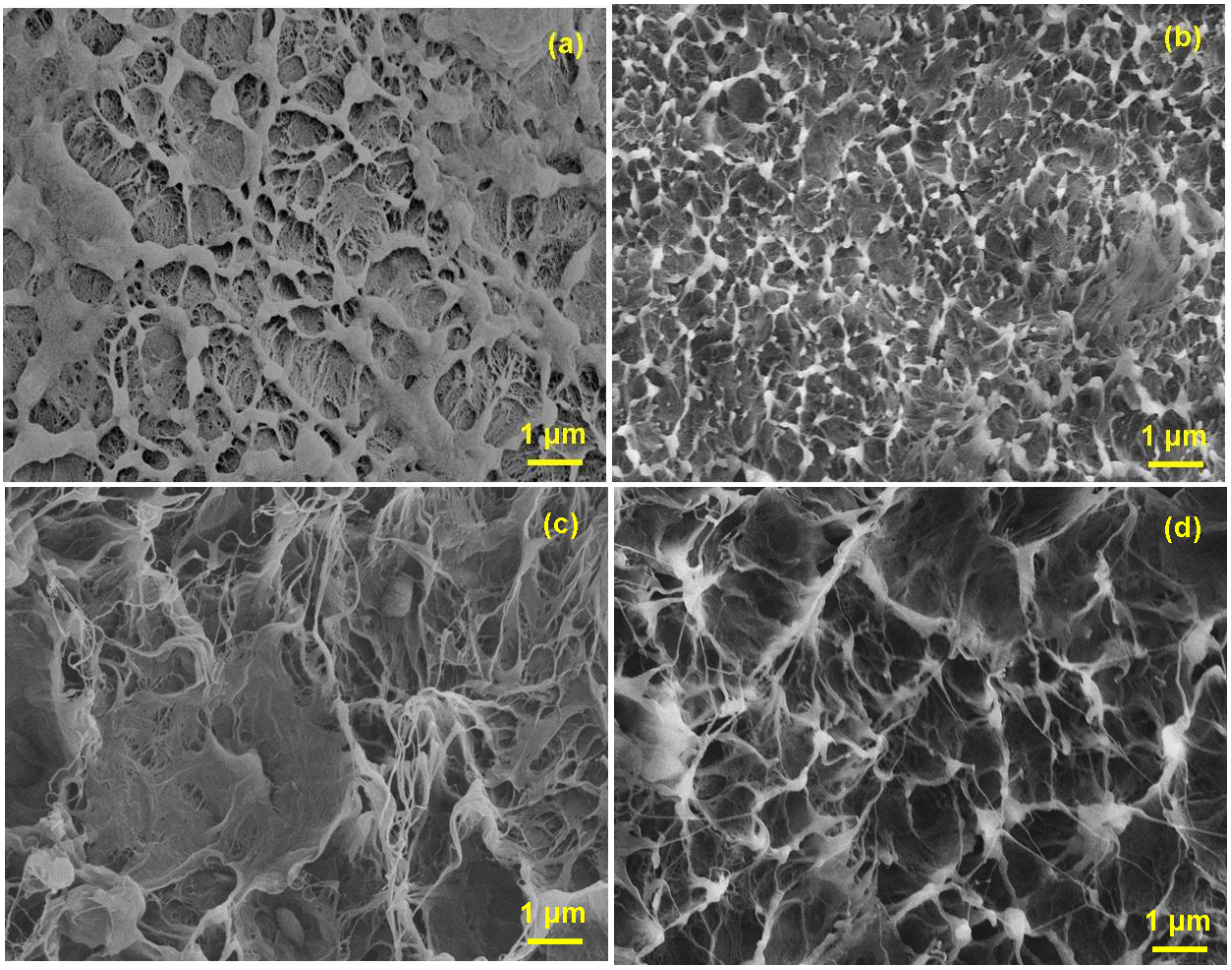

**Fig. 8**

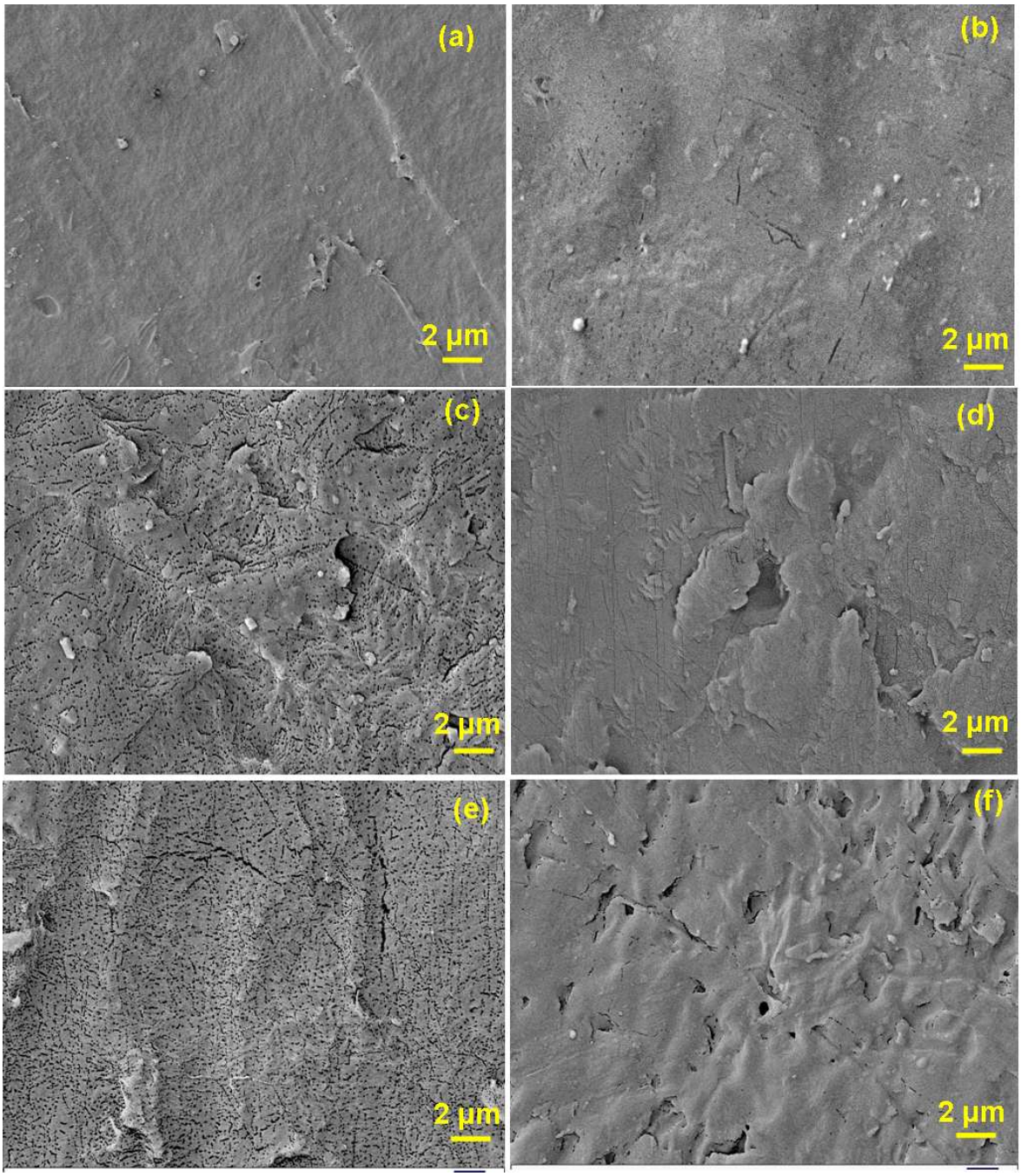

**Fig. 9**

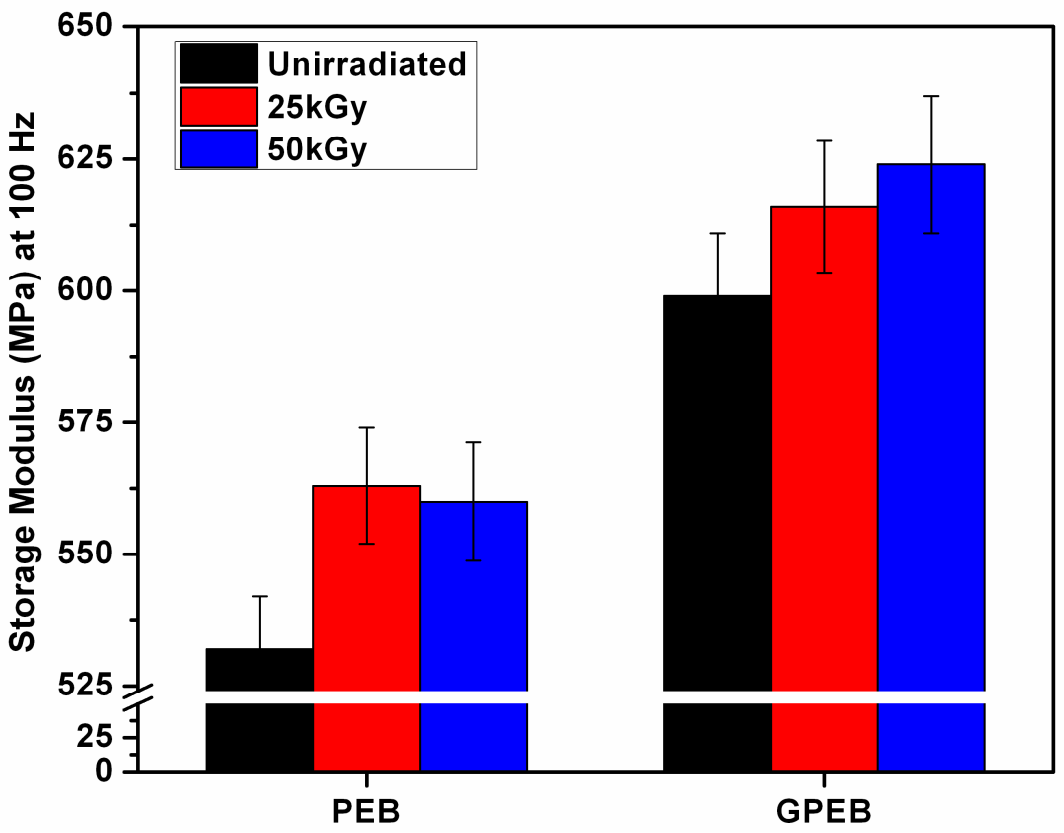

**Fig. 10**